A Review of the Mechanical Properties of Materials Used in Nb_3Sn Magnets for Particle Accelerators

G. Vallone, E. Anderssen, B. Bordini, P. Ferracin

***Abstract*—Superconducting magnets experience significant thermo-mechanical loads throughout their life cycle. These are introduced by the electro-magnetic forces during powering, but also by the prestress applied in many magnet designs. Further to this, the large thermal excursion that components of different materials experience can generate significant i nternal forces. The loads are also experienced by the superconducting coils, whose critical current can decrease as a consequence of the applied strain. It is then crucial to predict the overall mechanical behavior and conservatively design a magnet, avoiding failure of the mechanical components and of the superconducting coils. Finite Element Analysis (FEA) is generally used to perform these tasks, but its results rely heavily on the material properties and models used. This is in particular true for the coil composite, which is simplified to allow reasonable model sizes in full magnet models. In this paper, we present the state-of-art knowledge of the mechanical properties of the materials mostly used in superconducting magnet construction. We review elastic and plastic properties at room and cryogenic temperature, thermal contraction, and summarize the state-of-art failure criteria for these materials. Finally, the paper summarizes the present understanding of the mechanical behavior and limits of Nb_3Sn coils. For the first time, an orthotropic failure criteria is proposed.**

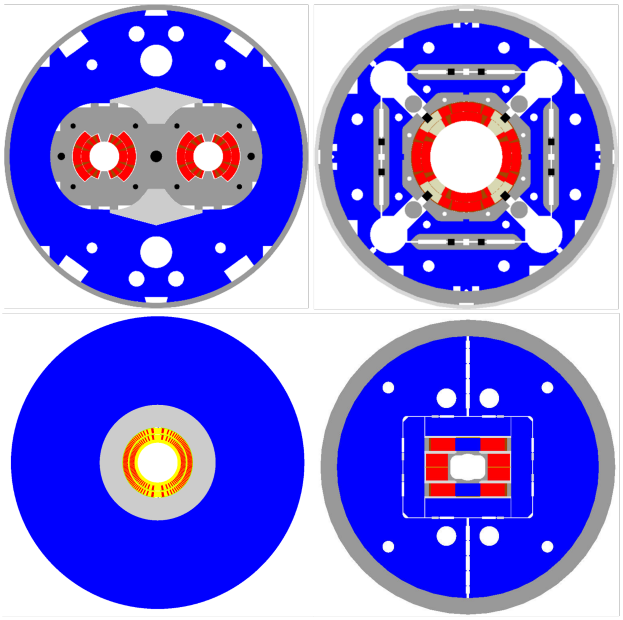

Fig. 1. Four cross-sections representing different magnet designs: a collared Cos(ϑ), the LHC main bending dipole (top left) [1], a bladder & key Cos(2ϑ) [2], MQXF (top right), a Canted Cos(ϑ) dipole (bottom left) [3], and a block design, the Test Facility Dipole (bottom right) [4].

I. Introduction

SUPERCONDUCTING magnets for particle accelerators typically use stiff mechanical structures to absorb the e.m. forces and apply a prestress that can prevent large conductor motions. Few examples of typical magnet cross sections are provided in Fig. 1. This small selection highlights the large range of materials used in these constructions. In all cases, the magnet is largely made out of a ferromagnetic steel (iron) [1]–[4]. In bladder and key designs [5], a thick aluminium shell is used to prestress the superconducting coils. Stainless steel is used for collars of collared designs, coil end spacers, plates/spacers in block designs, and liquid helium containment vessels. High strength steels are used in certain designs for collars, high strength bolts, or for end plates that react to the longitudinal e.m. forces. Aluminium bronze components are typically used in coil spacers (cos(ϑ design), or rails (block designs). For Canted Cos(ϑ) magnets, the entire mandrel is made of aluminium bronze. This material selection is mostly due to its ability to closely match the thermal contraction of the cable, in turn reducing potential issues during the reaction of the Nb_3Sn conductor to 650 °C. Plastics (e.g. Kapton), are used as insulator. Often, insulating layers can also be used as shims, allow to accommodate errors in the coil size. Glass Fiber Reinforced Plastics (GFRP) are used as cable insulation, but also as alignment keys or spacers. Some cable designs use mica layers as additional insulator, since the high resistivity of this material can reduce the insulation thickness.

The mechanical design of these objects was performed either with analytical formulas, or on 2D and 3D finite element models. The performance of these models (and of the design) are strongly dependent on the correct knowledge of the material properties. The key properties for magnet design are the elastic behaviour of the components, their thermal contraction up to cryogenic temperatures, and their strength. Unfortunately, it is often difficult to collect the necessary data for the materials, and sometime confusing criteria were used to verify the structural soundness. In this paper, we try to review the available data, and to discuss the state-of-the-art criteria available to verify the components. Materials are divided in three different typologies: ductile metals, brittle metals, composites. The Nb_3Sn coil composite is treated separately: after discussing elastic and elasto-plastic modeling strategies and related properties, we propose a 3D limit criterion to prevent filament breakage and bonding failure.

This work was supported by the U.S. LHC Accelerator Research Program. G. Vallone, E. Anderssen and P. Ferracin are with Lawrence Berkeley National Laboratory, Berkeley, CA 94720 USA

(e-mail: gvallone@lbl.gov).

TABLE I
SUPERCONDUCTING MAGNETS MATERIAL PROPERTIES

Material	Details	Room Temperature E GPa	σ_y MPa	R_m MPa	δ %	K_{Ic} MPa$\sqrt{m}$	S_m MPa	4.5 K E MPa	σ_y MPa	R_m MPa	δ MPa	K_{Ic} MPa$\sqrt{m}$	FAD MPa	S_m MPa	ν /	T.C. mm/m
Titanium[1]	Grade V, ⊥	118	830	900		100	692	126	1643	1673		58	976	813	0.3	1.7
	Grade V, ∥	126						135								
Aluminium[2]	A7075	70	480				400	79	490	650		25	412	343	0.33	4.2
Magnetic Steel[3]	Armco	224	210	286			175	213		975		25	437	364	0.3	2
Magnetic Steel[3]	Magnetil	200	115	249			96	200		723		30			0.3	2
Stainless Steel[4]	SS316LN	193	238	565			198	210	610	1455				508	0.28	2.95
	∥	30	257				214	30	496					413	0.3	2.44
G10[5]	⊥ tens.	5.6	20				17	5.6	20					17	0.3	7.06
	⊥ compr.		420				350		749					624		
Nitronic 40[6]		225	682	889	31	>438	568	210	1427	1813	11	118		1189	0.3	2.6
ODS Copper[7]	C3/30	110	270	350	13		225	110	340	540	20			283	0.3	3.1
Aluminum Bronze[8]	C61400	109	410	574	40		342	112	568	927	52			473	0.3	3.12
Aluminum Bronze[9]	C63000							133	578	918	6.2			482		
Aluminum Bronze[10]	C64200	109	197	556	64		164	130	306	758	70			255		
Phosphor Bronze[10]	C52100	113	122	321	60		102	126	247	578	75			206		
Phosphor Bronze[10]	C51000	110	147	360	72		123	132	315	639	66			263		

[1] [6]–[8], [2] [9], [10], [3] [11]–[13], [4] [7], [14], [5] [7], [6] [7], [14]–[16], [7] [17], [18], [8] [9], [9] [19], [10] [20]

II. MATERIAL PROPERTIES REVIEW

A collection of useful mechanical properties for materials commonly used in superconducting magnets can be found in Table I. The references used for each material are reported on the bottom of the table. The properties provided are the elastic modulus E, the yield strength σ_y, the material strength R_m, the elongation δ, and the fracture toughness K_{IC}. The latter can be orientation dependant; only the lowest value is reported. Finally, a value for the maximum allowable stress S_m is reported. The definition of S_m is a function of the material typology (ductile/brittle/composite), and the reader should refer to Section III for more details. Properties are provided at room temperature and at cold (4.5 K). The thermal contraction and Poisson's coefficient are in separate columns - the latter can actually be a function of the temperature, but measurements at cryogenic temperatures are not available for most (or all) the materials considered. Some of the spaces are left blank. This is either because the corresponding data value was not found; or because is not important (e.g. toughness of ductile metals).

A. Thermal Contraction

In magnet design, it is of great importance to predict correctly the interactions due to the differential thermal contraction of different materials. Because of the large temperature change, enormous forces can be exchanged by the structural components during the cooldown to cryogenic temperatures. The thermal contraction as a function of the temperature for various materials is shown in Fig. 2, top. The data was extracted from the NIST database [21]. Even if the lines seem unrelated, the percentage of dimensional change as a function of the temperature is very close to constant for the materials of interest (Fig. 2), bottom). The error range for the materials considered is below 8%. This is a great advantage in modeling, as it is possible, even if the properties are non-linear, to simulate the cooldown assuming a linear scaling with respect to the temperatures. In practical terms, this means that the designer can use a single value for the secant thermal contraction.

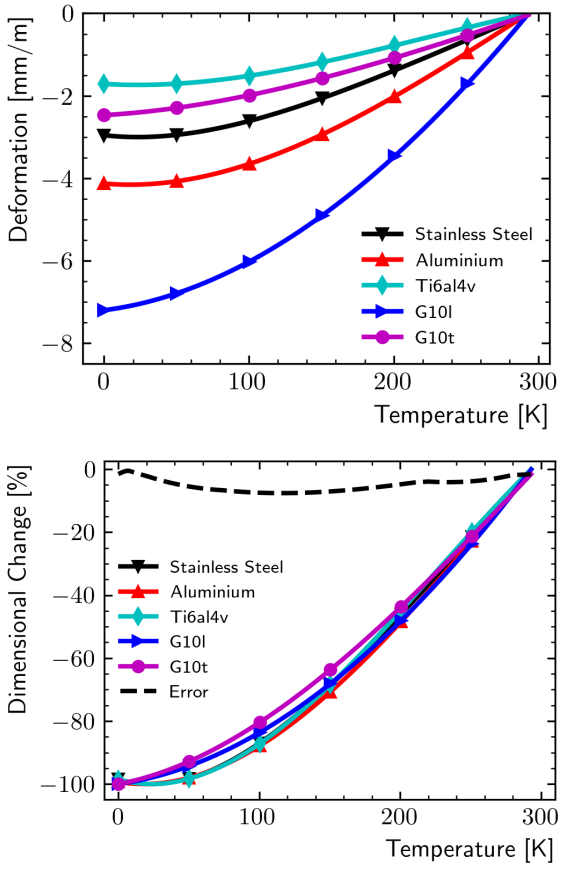

Fig. 2. Thermal contraction of various materials (top), and dimensional change % (bottom), as a function of the temperature.

B. Composites

Glass fiber reinforced plastics are used in magnets as wedges [22], spacers [2], or insulation [2]. The mechanical

properties of these materials depend strongly from the production process, and should be computed for each component. Of particular interest for magnets is the evaluation of the stiffness of braided glass fiber insulation. An estimate can be obtained assuming that the braid is a lay-up of two laminae. For each lamina, an $[E]$ tensor can be derived from micro-mechanics considerations (see [23]). The laminate properties in the fiber plane can be computed assuming a $(\pm\phi)$ stack, where ϕ is the braid angle [23]. The transverse properties for the laminate are similar to the lamina ones.

III. Design Criteria

Stress limits are imposed on the design to ensure that the components will not fail under the applied loads. Hereafter, we report the state-of-art criteria used for magnet design. The stress limits are reported in Table I, where the design strength S_m is computed assuming a safety/load factor of 1.2 for ductile materials or fragile materials respectively.

A. Ductile Metals

Ductile metals are used, for example, in aluminium bronze wedges [24]; bronze CCT mandrels [3]; soft aluminium collars [24], stainless steels for collars, spacers and rods [1], [4]; high strength steels for end loading systems [24]. They are typically verified against the Von Mises equivalent stress, slightly less conservative than the Tresca criterion. The Von Mises stress σ_{vm} is scalar in nature, and is related to the second tensor invariant of the deviatoric component of the stress tensor:

$$\sigma_{vm}^2 = \frac{1}{2}[(\sigma_{11}-\sigma_{22})^2 + (\sigma_{22}-\sigma_{33})^2 + (\sigma_{33}-\sigma_{11})^2 + 6(\sigma_{12}^2+\sigma_{23}^2+\sigma_{31}^2)] \quad (1)$$

Plastic deformation onset is avoided if the equivalent stress is lower than the yield stress σ_y. A safety factor $\sigma_{vm}/\sigma_y = 1.2$ is used to compute the allowable stress S_m in Table I.

B. Brittle Metals

A material is considered brittle when its toughness (K_{Ic}) is lower than 100 MPa·m$^{1/2}$. Examples of brittle metals used in magnets are iron yokes (ARMCO [11] and Magnetil); aluminum shells used in bladder and key constructions [HP]; titanium winding poles [2]. In many magnets designed in the past, only the iron was considered brittle, and was verified against an unclear limit on the maximum principal stress.

A more accurate alternative, proposed here, is to use the R6 method, developed for thick wall pressure vessels and piping for the Nuclear industry in the UK in the mid 1970's. The method defines a limit condition for the material in terms of a Failure Assessment Diagram (FAD) curve [25]–[27]. The first FAD diagram was derived from a modified version of the strip yield model [28], [29], and can be written as:

$$K_r(S_r) = S_r\left[\frac{8}{\pi^2}\ln\left(\sec\left(\frac{\pi}{2}S_r\right)\right)\right]^{-1/2} \quad (2)$$

where $K_r = K_I/K_{Ic}$ is a normalized stress intensification factor, $S_r = \sigma/\sigma_c$ the normalized stress, K_{Ic} the fracture

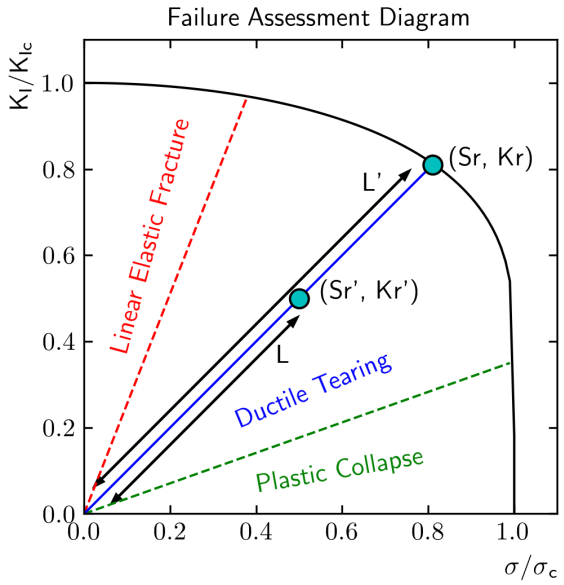

Fig. 3. Failure Assessment Diagram used to asses limits in brittle metals.

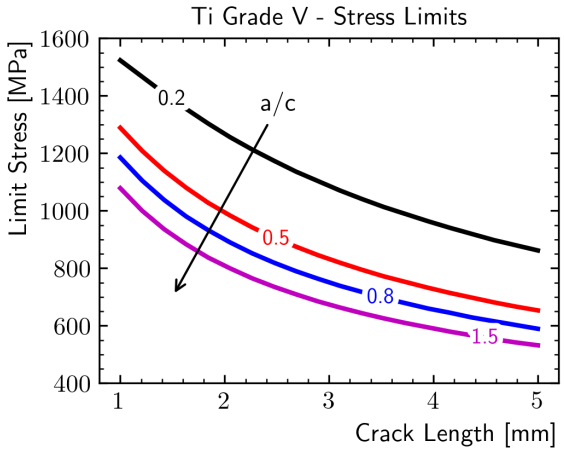

Fig. 4. Limit stress in grade V Titanium at 4.5 K, as a function of the crack length (a) and width (c).

toughness. σ_c is the 'collapse stress', assumed equal to the average between the material strength and the yield stress: $(R_m+\sigma_y)/2$. When K_r is equal to 0, the solution of Eq. 2 is larger than zero. In this region the failure line is completed assuming the collapse stress σ_c as limiting condition. The FAD, presented in Fig. 3, can capture the broad range of elastic fracture, ductile tearing, and plastic failure. Assessment (load) points (L) are characterized by a stress ratio S_r' and a stress intensity ratio K_I': when inside the FAD curve the design is safe from failure. The "Projected Load Point," (L') can be determined projecting the Load Point onto the limit curve [30]:

$$\phi = atan\left(\frac{K_r'}{S_r'}\right); \qquad S_r = \frac{2}{\pi}\,acos\left(e^{\frac{-(\pi\ cot(\phi))^2}{8}}\right) \quad (3)$$

The Load Factor ($\eta = L/L'$) is a measure of the load margin

for an object with a given flaw:

$$\eta = \sqrt{\frac{(S_r{}^2 + K_r{}^2)}{(S_r'{}^2 + K_r'{}^2)}} \tag{4}$$

η does not coincide with a safety factor, as flaws do not propagate along the load line L. The FAD selected here does not closely match the failure envelope near the plastic collapse region for materials with significant hardening [31]. This can be neglected for most high strength aluminium and magnetic steels used in Nb_3Sn magnets. However, it can be relevant for certain austenitic steels (e.g. Nitronic), for which different curves should be used to assess against plastic collapse (following for example the provisions from BS-7910 [26]). In magnet applications these materials are typically verified only against the yield stress, as described in Section III.a.

The FAD evaluation requires to extract the stress profile at the minimum stress gradient path starting from the flaw edge. This operation can be time consuming and poor suited for typical magnet design optimization studies, where many different design solutions are evaluated. Alternatively, one could conservatively assume a constant stress over the entire flaw, and take into account only the maximum between the equivalent stress and the first principal stress. The limit stress computed with the FAD with these assumptions, as a function of the crack length and width (a, c), is provided in Fig. 4 for a grade V titanium at 4.5 K. If the load is applied in a quasi-static fashion, we can also assume that the flaw will slowly propagate to a round shape. This allows to limit the analysis to the $a/c = 1$ line in Fig. 4. For a reference crack size of 1.5 mm, we then identify an 'FAD' value, reported in Table I, along with a limit stress S_m, obtained considering a load factor of 1.2. The value should be compared with the maximum between the Von Mises or first principal stress.

C. Composites

Composite materials can fail in multiple ways, e.g.: fiber breakage, matrix cracking, delamination, interlaminar shear. Laminated composites (e.g. insulation) are generally verified against the first ply failure load, defined as the the load at which the linear load-displacement curve first changes. Under this assumption, the laminate does not necessarily fail, as other undamaged plies can still carry the load, and the load at ultimate failure might be considerably higher. To compute the strength of each ply, different criteria are available, typically divided between non-interactive, interactive and physically based. The maximum strain and stress criteria [32], belonging to the first category, are respectively written as:

$$\begin{bmatrix} e_L^- < \varepsilon_1 < e_L^+ \\ e_T^- < \varepsilon_2 < e_T^+ \\ |\gamma_{12}| < g_{LT} \end{bmatrix}; \qquad \begin{bmatrix} s_L^- < \sigma_1 < s_L^+ \\ s_T^- < \sigma_2 < s_T^+ \\ |\tau_{12}| < t_{LT} \end{bmatrix} \tag{5}$$

where 1 is the fiber direction, and 2 the transverse one. The accuracy of these criteria under multi-axial loading conditions is limited. Better predictions in this regard can be obtained by quadratic interactive criteria as Tsai-Hill [33] or Tsai-Wu [34]:

TABLE II
Nb_3Sn COIL PROPERTIES

	Unit	R.T.			4.5 K		
		Elastic	Plastic	Avg.	Elastic	Plastic	Avg.
E_x	GPa	52.6	11.3	31.9	48.0	12.0	30.0
E_y	GPa	37.4	11.6	24.5	40.2	12.0	26.1
E_z	GPa	66.1	28.1	47.1	77.2	38.4	57.8
G_{xy}	GPa	18.8			17.7		
G_{yz}	GPa	19.8			22.5		
G_{xz}	GPa	22.9			24.1		
ν_{xy}	/	0.19			0.24		
ν_{yz}	/	0.17			0.16		
ν_{xz}	/	0.23			0.18		
α_x	mm/m	3.65					
α_y	mm/m	4.03					
α_z	mm/m	2.33					

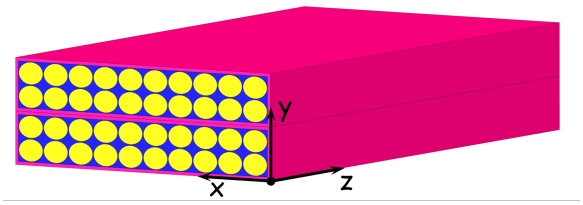

Fig. 5. Coil reference system. In Cos(ϑ) designs, the x, y and z directions correspond respectively to the radial, azimuthal and longitudinal ones.

$$\frac{\sigma_1^2}{s_L^2} - \frac{\sigma_1\sigma_2}{s_L^2} + \frac{\sigma_2^2}{s_T^2} + \frac{\tau_{12}}{t_{LT}^2} < 1; \tag{6}$$

$$F_{11}\sigma_1^2 + F_{22}\sigma_2^2 + F_{66}\tau_{12}^2 + F_1\sigma_1 + F_2\sigma_2 + 2F_{12}\sigma_1\sigma_2 < 1 \tag{7}$$

Finally, physically based criteria express multi-axial limits as a function of different failure modes (e.g. Hashin [35], [36], Puck [37], LaRC [38], [39]). Of particular interest for magnet design are matrix failures under compressive loads transversal to the fibers. In particular, it was found in [40] that quadratic criteria can be inadequate to predict failures under confining pressure. The Mohr-Coulomb theory, used in many of these physically based criteria, predicts failure occurs for any stress state whose Mohr circle is tangent to the Mohr-Coulomb fracture line, and can be written as [39]:

$$\tau_{fp} = s - \eta\sigma_n \quad \text{where:} \quad \tan(2\alpha_0) = -1/\eta \tag{8}$$

where τ_{fp} is the shear stress acting on a potential failure plane; σ_n is the normal traction; η a friction coefficient related to the failure plane angle α_0 (equal to 53° for most composite materials [38].)

IV. SUPERCONDUCTING COILS

A. Stiffness

The stiffness of Nb_3Sn coils is measured on stacks of impregnated cables. Many of these measurements were performed in the past, using various experimental set-ups and cable geometries [41]. However, published results differ substantially, making it challenging to select the *correct* value. In

TABLE III
Nb_3Sn COIL STRENGTH LIMITS

	Unit	R.T.		4.5 K	
		Compression	Tension	Compression	Tension
e_L	%	-1.1	0.25	-1	0.35
s_T	MPa	-175	20	-150	20
t_{LT}	MPa	20		20	

reality, the actual properties of the coil are a function of the overall cable design, and should be computed on each design as for other composite materials. This process can be time consuming, and not adoptable in early design studies, when the cable geometry is not well defined. 'Generic' properties are then required. In the past, the coil was assumed as elastic, with a transverse modulus of 44 GPa [24]. However, it was shown in [2] that a significantly lower value (20 GPa) was required to match the measured magnet behavior. The significant difference between this result and the earlier assumptions was likely due to different interpretations of the coil non-linear behavior, due to the early on-set of plasticity in the copper matrix [42]. In particular, past authors were using the 'unloading' modulus, while in most situation the load in the coil increases, making the tangent modulus a preferred choice. Elasto-plastic models [43] can be more accurate for simulating cycling behaviour. Using the modeling strategy proposed in [42], an MQXF cable stack was tested under loads in all directions. Results are provided in Table II, where E_i represents the Young's modulus in the i-th direction, ν_{ij} the Poisson coefficient, α_i the integral thermal contraction from room temperature to 1.9 K. The directions x, y, z are defined following the reference system shown in Fig. 5. We also provide an 'average' between the elastic and plastic behavior, which can be useful for quick computations.

B. Strength

Nb_3Sn coils can fail in many ways: filament cracking/failure, insulation damage, epoxy cracking, insulation debonding. Their critical current is also a function of the applied strain [43]. Failure in the coil composite may not result in a reduction of performances. For example, detachment between coil and insulation can be tolerated [44]. Because of this, an univocal definition of 'strength' for Nb_3Sn coils does not exist: it could be any failure of any part of the composite, or anything that would reduce magnet performance. Consequently, it has been difficult to establish a clear design criterion. Currently, the coils are verified against the Von Mises stress, computed assuming an uniform elastic material model. This approach is a result of consistent comparison between magnet tests and computations [45]. However, it cannot be used with more advanced modeling strategies and material models, and it is not coherent with typical failure criteria used in composite mechanics.

Here an orthotropic failure criterion, based on mixed maximum stress-strain limits, is proposed. In this exercise the failure is defined as a reduction of the current-carrying capability of the strand/cable, and the limits are extracted from the available experiments where this reduction was measured. No physical consideration on the failure mode at the filament level is made in this definition. The selected measurements, performed on superconducting strands and Rutherford cables, have allowed to probe the coil limits under a variety of uniaxial loading conditions. The criterion is non-interactive, since no clear failure tests under multi-axial conditions exist, and is defined as follows:

$$\begin{bmatrix} e_L^- < \varepsilon_1 < e_L^+ \\ s_T^- < \sigma_2 < s_T^+ \\ |\tau_{12}| < t_{LT} \end{bmatrix} \tag{9}$$

where 1 is the strand axis, and 2 the transverse one. Measurements on Rutherford cables under transverse loading allowed to measure a compressive limit s_T^-. At room temperature, a limit of 175 MPa was measured [46]; some irreversible critical current reduction was measured at 150 MPa at cryogenic temperatures [42]. Reasonably, this limit should not change too much when rotating the load in the cross-sectional plane. The limit is also in reasonable agreement with results from multiscale numerical models [43]. The longitudinal limits $e_L^+,\ e_L^-$ can be measured with Walter-spring measurements on strands [47]–[49]. Failure in shear t_{LT} and transverse tension s_T^+ is likely connected to internal debonding, and can be measured with dedicated tests [50]. The strength limits are reported in Table III. Further to this, bonds between the coil and other components can fail. Their progressive failure can be included in numerical models with cohesive elements [44]. The reported limits are potentially non-conservative, and based on failure measurements with low or no statistics. On the other hand, it is possible that the real limits might be higher under multiaxial stress conditions, especially under compressive loads.

V. CONCLUSION

This paper is an attempt at providing all the mechanical properties necessary to design a Nb_3Sn superconducting magnet. We have highlighted how the percentage of thermal contraction, as a function of the temperature, does not change for the materials of interest. The state-of-art of magnets design criteria for metal and composite components was described. Finally, we proposed an orthotropic elasto-plastic model and failure criterion for Nb_3Sn coils, built on available experimental data.

REFERENCES

[1] L. Rossi, "The LHC main dipoles and quadrupoles toward series production," *IEEE Transactions on Applied Superconductivity*, vol. 13, no. 2, pp. 1221–1228, 2003. DOI: 10.1109/TASC.2003.812639.

[2] G. Vallone *et al.*, "Mechanical performance of short models for MQXF, the Nb_3Sn low-beta quadrupole for the Hi-Lumi LHC," *IEEE Transactions on Applied Superconductivity*, vol. 27, no. 4, 2016. DOI: 10.1109/TASC.2016.2645133.

[3] S. Caspi *et al.*, "Design of a Canted-Cosine-Theta superconducting dipole magnet for future colliders," *IEEE Transactions on Applied Superconductivity*, vol. 27, no. 4, 2017. DOI: 10.1109/TASC.2016.2638458.

[4] G. Vallone *et al.*, "Magnetic and mechanical analysis of a large aperture 15 T cable test facility dipole magnet," *IEEE Transactions on Applied Superconductivity*, vol. 31, no. 5, 2021. DOI: 10.1109/TASC.2021.3065882.

[5] S. Caspi *et al.*, "The use of pressurized bladders for stress control of superconducting magnets," *IEEE Transactions on Applied Superconductivity*, vol. 11, no. 1 II, pp. 2272–2275, 2001. DOI: 10.1109/77.920313.

[6] M. Reytier, F. Kircher, and B. Levesy, "Characterization of titanium alloys for cryogenic applications," *AIP Conference Proceedings*, vol. 614, no. 1, pp. 76–83, 2002. DOI: 10.1063/1.1472528.

[7] *Matweb, material property data*, https://www.matweb.com.

[8] J. K. Childs and M. M. Lemcoe, "Determination of materials design criteria for 6Al-4V titanium alloy at room and elevated temperatures. period covered Junuary 1956 to May 1958," English, Southwest Research Inst., San Antonio, Tech. Rep. WADC-TR-58-246, 1958.

[9] H. J. Hucek, K. E. Wilkes, K. R. Hanby, and J. K. Thompson, "Handbook on materials for superconducting machinery, includes data sheets for first and second supplements, November 1975 and January 1977," Battelle Columbus Labs Ohia Metals and Ceramics Information Center, Tech. Rep., 1977.

[10] H. Pan *et al.*, "Fracture failure analysis for MQXFA magnet aluminum shells," *IEEE Transactions on Applied Superconductivity*, vol. 30, no. 4, 2020. DOI: 10.1109/TASC.2020.2972230.

[11] I. A. Santillana *et al.*, "Mechanical characterization of low-carbon steels for high-field accelerator magnets: Application to Nb_3Sn low-β quadrupole MQXF," *IEEE Transactions on Applied Superconductivity*, vol. 32, no. 6, 2022. DOI: 10.1109/TASC.2022.3149853.

[12] F. Bertinelli, F. Fudanoki, T. Komori, G. Peiro, and L. Rossi, "Production of austenitic steel for the LHC superconducting dipole magnets," *IEEE Transactions on Applied Superconductivity*, vol. 16, no. 2, pp. 1773–1776, 2006. DOI: 10.1109/TASC.2006.873244.

[13] A. Portone *et al.*, "Design and optimization of the 12.5t efda dipole magnet," en, *Cryogenics*, This issue contains papers from CHATS-2005: Workshop on Computation of Thermohydraulic Transients in Superconductors, vol. 46, no. 7, pp. 494–506, 2006. DOI: 10.1016/j.cryogenics.2006.01.011.

[14] C. L. Goodzeit, "Superconducting accelerator magnets - an introduction to mechanical design and construction methods," *USPAS, January 2001*, 2001.

[15] R. P. Walsh, K. J. Radcliff, J. Lu, and K. Han, "The low temperature mechanical properties of a Nitronic 40 forging," en, *IOP Conference Series: Materials Science and Engineering*, vol. 756, no. 1, p. 012001, 2020. DOI: 10.1088/1757-899X/756/1/012001.

[16] F. R. Fickett and R. P. Reed, "Materials studies for magnetic fusion energy applications at low temperatures- i," en, National Bureau of Standards, Gaithersburg, MD, Tech. Rep. NBS IR 78-884, 1978, NBS IR 78–884.

[17] J. Arnaud, "ODS Copper Discup C3/30 thermal expansion, note SBT/CT12-28," INAC 2021, Tech. Rep., 2021.

[18] D. Smekens, "Characterization of discup C3/30 ODS copper alloy for 11T DS dipole from luvata OY/ECKA granules. available on EDMS," CERN, Tech. Rep., 2012.

[19] M. Crouvizier, "C63000 alloy – tensile properties at 4.2K, EDMS no. 2022573," CERN, Tech. Rep., 2018.

[20] M. Crouvizier, "Copper alloys for wedges of 16T magnets, CERN, 2018, EDMS no. 1959720," CERN, Tech. Rep., 2018.

[21] *NIST, properties of solid materials*, https://www.trc.nist.gov/.

[22] A. Louzguiti *et al.*, "Optimization of the electromagnetic design of the FCC sextupoles and octupoles," *IEEE Transactions on Applied Superconductivity*, vol. 29, no. 5, 2019. DOI: 10.1109/TASC.2019.2892839.

[23] L. P. Kollár and G. S. Springer, *Mechanics of Composite Structures*, en. Cambridge University Press, 2003.

[24] M. Juchno *et al.*, "Support structure design of the Nb_3Sn quadrupole for the High Luminosity LHC," *IEEE Transactions on Applied Superconductivity*, vol. 25, no. 3, pp. 1–4, 2015. DOI: 10.1109/TASC.2014.2366034.

[25] R. P. Harrison, I. Milne, and T. G. F. Gray, "Assessment of defects: The c.e.g.b. approach [and discussion]," *Philosophical Transactions of the Royal Society of London. Series A, Mathematical and Physical Sciences*, vol. 299, no. 1446, pp. 145–153, 1981.

[26] "The british standards institute, guide to methods for assessing the acceptability of flaws in metallic structures, BS 7910:2013," The British Standards Institute, Tech. Rep., 2013.

[27] T. L. Anderson, *Fracture mechanics: fundamentals and applications*. CRC press, 2017.

[28] D. Dugdale, "Yielding of steel sheets containing slits," *Journal of the Mechanics and Physics of Solids*, vol. 8, no. 2, pp. 100–104, 1960. DOI: 10.1016/0022-5096(60)90013-2.

[29] G. Barenblatt, "The mathematical theory of equilibrium cracks in brittle fracture," in ser. Advances in Applied Mechanics, H. Dryden, T. von Kármán, G. Kuerti, F. van den Dungen, and L. Howarth, Eds., vol. 7, Elsevier, 1962, pp. 55–129. DOI: 10.1016/S0065-2156(08)70121-2.

[30] J. Bloom, "Prediction of ductile tearing of compact fracture specimens using the R-6 failure assessment diagram," *International Journal of Pressure Vessels and Piping*, vol. 8, no. 3, pp. 215–231, 1980. DOI: 10.1016/0308-0161(80)90026-5.

[31] I. Milne, "Failure assessment diagrams and j estimates: A comparison for ferritic and austenitic steels," *International journal of pressure vessels and piping*, vol. 13, no. 2, pp. 107–125, 1983.

[32] S. Tsai and H. T. Hahn, *Introduction to Composite Materials*. Technomic Publishing Co. Inc., 1980. DOI: 10.1201/9780203750148.

[33] S. W. Tsai, "Strength theories of filamentary structure," *Fundamental aspects of fiber reinforced plastic composites*, 1968.

[34] S. W. Tsai and E. M. Wu, "A general theory of strength for anisotropic materials," *Journal of Composite Materials*, vol. 5, no. 1, pp. 58–80, 1971. DOI: 10.1177/002199837100500106.

[35] Z. Hashin and A. Rotem, "A fatigue failure criterion for fiber reinforced materials," *Journal of Composite Materials*, vol. 7, no. 4, pp. 448–464, 1973. DOI: 10.1177/002199837300700404.

[36] Z. Hashin, "Fatigue Failure Criteria for Unidirectional Fiber Composites," *Journal of Applied Mechanics*, vol. 48, no. 4, pp. 846–852, Dec. 1981. DOI: 10.1115/1.3157744.

[37] A. Puck and W. Schneider, "On failure mechanisms and failure criteria of filament-wound glass-fibre/resin composites," *Plastics and Polymers*, vol. 37, no. 127, pp. 33–43, 1969.

[38] S. T. Pinho, C. G. Dávila, P. P. Camanho, L. Iannucci, and P. Robinson, "Failure models and criteria for frp under in-plane or three-dimensional stress states including shear non-linearity," NASA, Tech. Rep. NASA/TM-2005-213530, 2005.

[39] S. Pinho, R. Darvizeh, P. Robinson, C. Schuecker, and P. Camanho, "Material and structural response of polymer-matrix fibre-reinforced composites," *Journal of Composite Materials*, vol. 46, no. 19-20, pp. 2313–2341, 2012. DOI: 10.1177/0021998312454478.

[40] J. P. Boehler and J. Raclin, "Failure criteria for glass-fiber reinforced composites under confining pressure," *Journal of Structural Mechanics*, vol. 13, no. 3-4, pp. 371–393, 1985. DOI: 10.1080/03601218508907506.

[41] C. Fichera *et al.*, "New methodology to derive the mechanical behavior of epoxy-impregnated Nb_3Sn cables," English, *Ieee Transactions on Applied Superconductivity*, vol. 29, no. 7, 2019. DOI: 10.1109/TASC.2019.2905224.

[42] G. Vallone, B. Bordini, and P. Ferracin, "Computation of the reversible critical current degradation in Nb_3Sn Rutherford cables for particle accelerator magnets," *IEEE Transactions on Applied Superconductivity*, vol. 28, no. 4, 2018. DOI: 10.1109/TASC.2018.2810222.

[43] G. Vallone *et al.*, "A methodology to compute the critical current limit in Nb_3Sn magnets," *Superconductor Science and Technology*, vol. 34, no. 2, 2020. DOI: 10.1088/1361-6668/abc56b.

[44] G. Vallone and P. Ferracin, "Modeling coil-pole debonding in Nb_3Sn superconducting magnets for particle accelerators," *IEEE Transactions on Applied Superconductivity*, vol. 27, no. 8, 2017. DOI: 10.1109/TASC.2017.2759249.

[45] H. Felice *et al.*, "Performance of a Nb_3Sn quadrupole under high stress," vol. 21, no. 3, pp. 1849–1853, 2011.

[46] P. Ebermann *et al.*, "Irreversible degradation of Nb_3Sn Rutherford cables due to transverse compressive stress at room temperature," en, *Superconductor Science and Technology*, vol. 31, no. 6, p. 065 009, 2018. DOI: 10.1088/1361-6668/aab5fa.

[47] N. Cheggour *et al.*, "Influence of Ti and Ta doping on the irreversible strain limit of ternary Nb_3Sn superconducting wires made by the restacked-rod process," *Superconductor Science and Technology*, vol. 23, no. 5, p. 052 002, Apr. 2010. DOI: 10.1088/0953-2048/23/5/052002.

[48] B. Bordini, P. Alknes, L. Bottura, L. Rossi, and D. Valentinis, "An exponential scaling law for the strain dependence of the Nb_3Sn critical current density," *Superconductor Science and Technology*, vol. 26, no. 7, p. 075 014, 2013. DOI: 10.1088/0953-2048/26/7/075014.

[49] N. Cheggour, T. C. Stauffer, W. Starch, L. F. Goodrich, and J. D. Splett, "Implications of the strain irreversibility cliff on the fabrication of particle-accelerator magnets made of restacked-rod-process Nb_3Sn wires," en, *Scientific Reports*, vol. 9, no. 1, p. 5466, 2019. DOI: 10.1038/s41598-019-41817-7.

[50] S. Krave, T. Shen, and A. Haight, "Exploring new resin systems for Nb_3Sn accelerator magnets," en, *IEEE Transactions on Applied Superconductivity*, vol. 31, no. 5, 2021. DOI: 10.1109/TASC.2021.3059607.